An [Fe^{III}_8] molecular oxyhydroxide

Daniel J Cutler,[a] Marco Coletta,[a] Mukesh K. Singh,[a] Angelos B. Canaj,[a] Laura J. McCormick,[b] Simon J. Coles,[b] Jürgen Schnack*[c] and Euan K. Brechin*[a]

[a]*EaStCHEM School of Chemistry, The University of Edinburgh, David Brewster Road, Edinburgh, Eh9 3FJ, Scotland, UK. E-mail: E.Brechin@ed.ac.uk*

[b]*EPSRC National Crystallography Service, School of Chemistry, University of Southampton, Highfield, Southampton, SO17 1BJ, UK.*

[c]*Universitat Bielefeld, Postfach 100131, D-33501 Bielefeld, Germany. Email: jschnack@uni-bielefeld.de*

Abstract

An [Fe^{III}_8] hexagonal bipyramid, which represents an all ferric piece of molecular magnetite, displays antiferromagnetic exchange between the two capping tetrahedral ions and the six ring octahedral ions resulting in a spin ground state, S = 10.

Introduction

Polymetallic complexes of Fe^{III} ion have always played a prominent role in the development molecular magnetism. [Fe^{III}_2] dimers,[1] [Fe^{III}_3] triangles[2] and [Fe^{III}_4] butterflies[3] not only represented ideal systems for developing quantitative magneto-structural correlations, they were also employed synthetically as starting materials for constructing larger and more complex species.[4] The latter often contain the same vertex-, edge-, face-sharing structural units as the reactants, linked via organic and inorganic bridging ligands. The large library of complexes produced therefrom allowed chemists to understand the processes by which larger clusters self-assemble, allowing some control over the resultant magnetic properties, targeting, for example, slow relaxation of the magnetisation,[5] spin frustration,[6] or an enhanced magnetocaloric effect.[7]

One interesting sub-set of species in this family are molecular iron oxides, an emerging class of materials whose structures, in the main, contain no bridging organic ligands and conform to mineral phases such as ferrihydrite and magnetite.[8] As well as displaying fascinating magnetic behaviours, such species potentially have applications in a breadth of areas ranging from catalysis[9] and battery technologies[10] to biomedical imaging.[11]

The striking structural similarties between the molecular iron oxides [Fe^{III}_{13}],[12] [Fe^{III}_{17}],[8,13] [Fe^{III}_{30}],[14] and [Fe^{III}_{34}][15] which all possess alternating "layers" or tetrahedral and octahedral Fe^{III} ions has prompted us to speculate, and examine, whether very large molecular iron oxides, perhaps even rivalling the size and complexity of the polyoxometalates,[15] can be isolated. The inability of Fe^{III} to be stabilised by terminal oxide ions and the propensity of aqueous solutions of Fe^{III} to produce mixtures of intractable/insoluble/amorphous solids suggests however that alternative synthetic pathways may have to be explored. The simplicity of the synthesis of [Fe_{17}] represents a good starting point. It is made by dissolving anhydrous $FeBr_3$ in wet pyridine.[8,13] The latter acts as solvent, base, source of oxide/hydroxide, terminal ligand and charge balancing counter cation (pyH^+). Analogous reactions replacing the pyridine with β-picoline, 4-ethylpyridine, isoquinolene, 3,4-lutidine, results in a series of isostructural species.[13] Addition of different bases, templates and solvent combinations results in the formation of the related, but larger [Fe_{30}] and [Fe_{34}] clusters.[14,15] Herein, we extend this methodology to the use of 4-methoxypyridine (MeO-py) and the synthesis of the smallest member of this molecular iron oxide family, an [Fe_8] cage.

Results and Discussion

Dissolution of $FeBr_3$ in MeO-py with stirring for 2.5 hours, followed by filtration and vapour diffusion with acetone results in the formation of orange plate-like crystals in 2 weeks. Crystals of $[Fe^{III}_8O_6(\mu\text{-}OH)_6(MeO\text{-}py)_{12}Br_2]Br_4{\cdot}3H_2O{\cdot}2MeO\text{-}py$ (**1**$\cdot$ $3H_2O{\cdot}2MeO\text{-}py$; Figure 1) are in a monoclinic crystal system and structure solution was performed in the space group *C*2/*c* (Table S1; Figure S1). The asymmetric unit contains half the formula. The metallic skeleton of **1** describes a hexagonal bipyramid, in which a ring of six octahedral Fe^{III} ions (Fe1-3 and symmetry equivalent, s.e.) is capped top and bottom by a tetrahedral Fe^{III} ion (Fe4 and s.e.). The tetrahedral Fe^{III} ions are linked to the $[Fe_6]$ ring through three $\mu_3\text{-}O^{2-}$ ions (O10, O20, O30 and s.e.), which further bridge two octahedral Fe ions around the inner rim of the wheel. The outer rim is bridged by six $\mu\text{-}OH^-$ ions (O1H, O2H, O3H and s.e.). The coordination sphere of the tetrahedral Fe ion is completed by the presence of a terminal Br^- ion (Br3 and s.e.), and those of the octahedral Fe ions by two MeO-py molecules. Fe-O-Fe bond angles fall in the ranges Fe(tet)-O-Fe(oct), 122.62-123.42°, and Fe(oct)-O-Fe(oct), 95.25-98.38°; note that the former are very much bigger than the latter. The Br^- counter anions (Br1, Br2 and s.e.) are H-bonded to the μ-OH ions (Br…O, 3.199-3.227 Å), as are the two MeO-py and three H_2O molecules of crystallization (Br…O, 3.365-3.674 Å; N…O, 2.847 Å; Figure S2). Closest inter-cluster interactions are between neighbouring MeO-py molecules at C/O…C/O distances ≥ 3.45 Å (Figure S3). The structural similarity between **1** and $[Fe_{17}]$ can be seen in Figure 2 in which the $[Fe_8]$ cation can be directly mapped onto half of the $[Fe_{17}]$ framework. The similarity between $[Fe_8]$ and $[Fe_{13}]$, $[Fe_{17}]$, $[Fe_{30}]$, $[Fe_{34}]$ and selected Fe minerals is shown in Figure S4. The hexagonal bipyramidal core is unique amongst the $[Fe_8]$ clusters reported in the Cambridge Structural Database, but the same unit exists in two $[Fe_{14}]$ clusters, $[Fe_{14}(bta)_6O_6(OMe)_{18}Cl_6]$ (where btaH = 1,2,3-benzotriazole) and $[Gd_{12}Fe_{14}O_{12}(OH)_{18}(tea)_6(CH_3COO)_{16}(H_2O)_8]$ (where H_3tea = triethanolamine), whose Fe metallic skeletons both describe hexacapped hexagonal bipyramids, albeit with the Fe ions all being octahedral.[7,17]

Magnetic measurements of **1** reveal strong antiferromagnetic interactions between the Fe^{III} ions. The experimental dc susceptibility data (*T* = 2-300 K, *B* = 0.1 T) for **1** are plotted in Figure 3 as the χT product versus *T*, where χ is the molar magnetic susceptibility, *T* is the temperature, and *B* the field. The value of χT at *T* = 300 K is ~38 cm^3 K mol^{-1}, larger than that expected for the sum of the Curie constants for eight Fe^{III} (*S* = 5/2) ions with g_{Fe} = 2.00 (35 cm^3 K mol^{-1}). As the temperature decreases, the magnitude of χT increases rapidly, reaching a maximum value of ~57 cm^3 K mol^{-1} at *T* = 16 K, where it then plateaus before decreasing slightly to a value of ~55 cm^3 K mol^{-1} at *T* = 2 K. The data are clearly indicative of a ferrimagnetic system, with the maximum in χT suggesting a ground state spin value of *S* = 10. This is corroborated by magnetisation data (*T* = 2-7 K, *B* = 0.5 – 7 T; Figure 3) which rise rapidly with increasing field strength and saturate just below *M* = 20 μ_B. Given the large discrepancy in the Fe(tet)-O-Fe(oct) and and Fe(oct)-O-Fe(oct) bond angles, the data suggest a strong antiferromagnetic interaction between the tetrahedral and octahedral Fe ions, analogous to that seen for $[Fe_{17}]$,[8,13] and consistent with published magneto-structural studies of O-bridged Fe^{III} compounds.[1] The magnetic data can be simulated using exact diagonalisation[18] and an isotropic spin-Hamiltonian $\hat{H} = -2\sum_{i<j} J_{ij}\hat{\vec{s}}_i \cdot \hat{\vec{s}}_j$ with a coupling scheme that assumes just two independent exchange interactions, J_{ring} and J_{cap}, describing the interaction between the octahedral ions in the $[Fe_6]$ wheel and between the tetrahedral and octahedral Fe ions, respectively (Figure 3). This affords J_{ring} = +4.475 cm^{-1} and J_{cap} = -17.376 cm^{-1} with *g* = 2.00. This results in a spin ground state, *S* = 10.

To further support the relative sign and magnitude of the exchange interactions obtained experimentally, we have performed DFT calculations on both dimeric and trimeric models derived from the full structure of **1** (Figures S6-7; see ESI for computational details).[19] This affords J_{ring} = +4.1

cm^{-1} and J_{cap} = -30.1 cm^{-1} for the dimeric model, and J_{ring} = +2.1 cm^{-1} and J_{cap} = -30.4 cm^{-1} for the trimeric model. We have also performed overlap integral calculations between the singly occupied molecular orbitals of the Fe^{III} ions.[19,20] These suggest three moderate magnetic orbital overlaps for J_{ring} resulting in small ferromagnetic interactions (Table S2, Figure S8a-c), and one strong and ten moderate magnetic orbital overlaps for J_{cap} leading to strong antiferromagnetic interactions (Table S2, Figure S8d-n). Spin density analysis indicates the presence of a strong spin delocalization mechanism, as seen previously for other polymetallic iron complexes (Figure S9).[20]

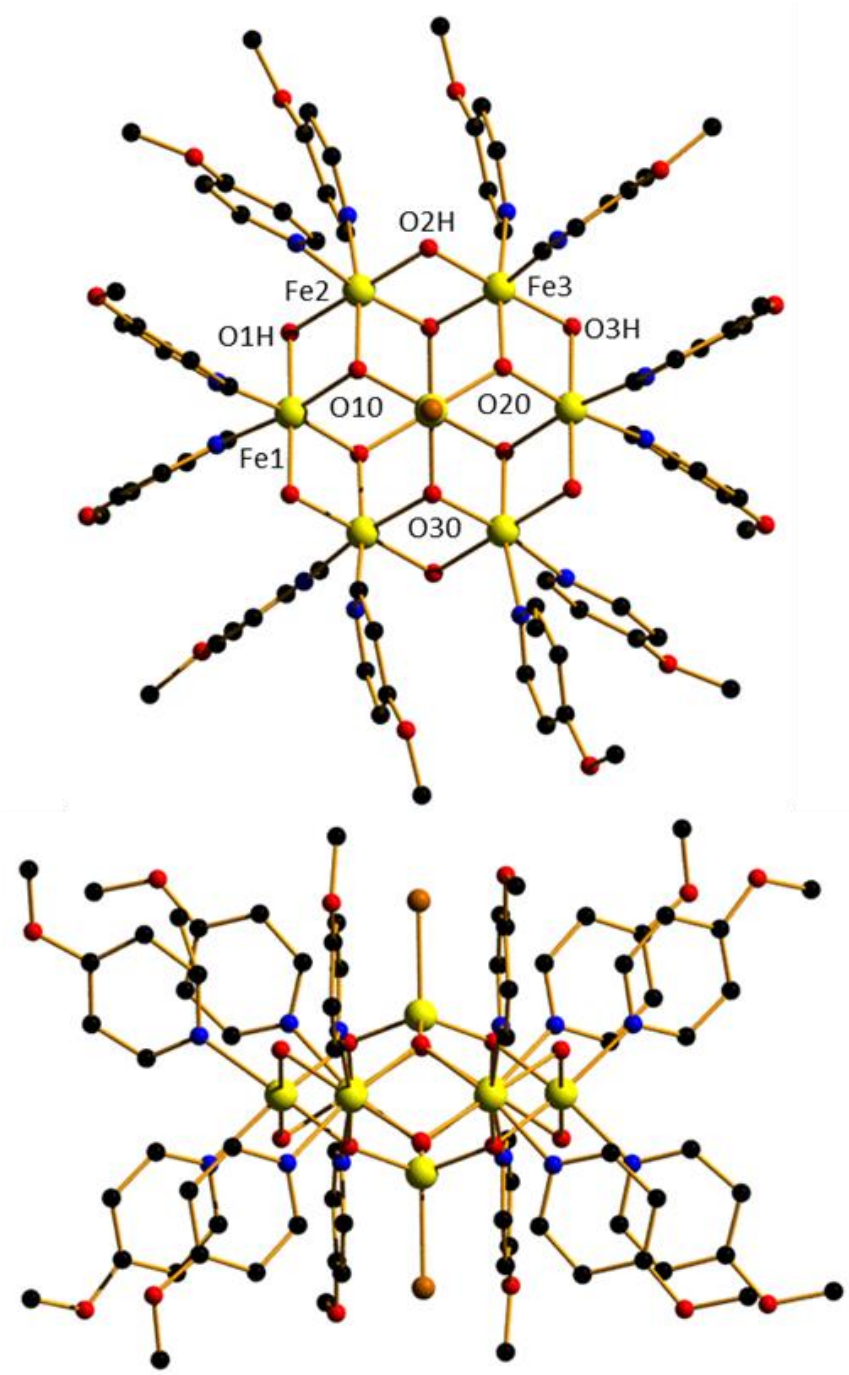

Fig.1 Orthogonal views of the molecular structure of the cation of **1**. Colour code: Fe = yellow, O = red, N = blue, Br = brown, C = black. H atoms, counter anions and solvent of crystallisation omitted for clarity.

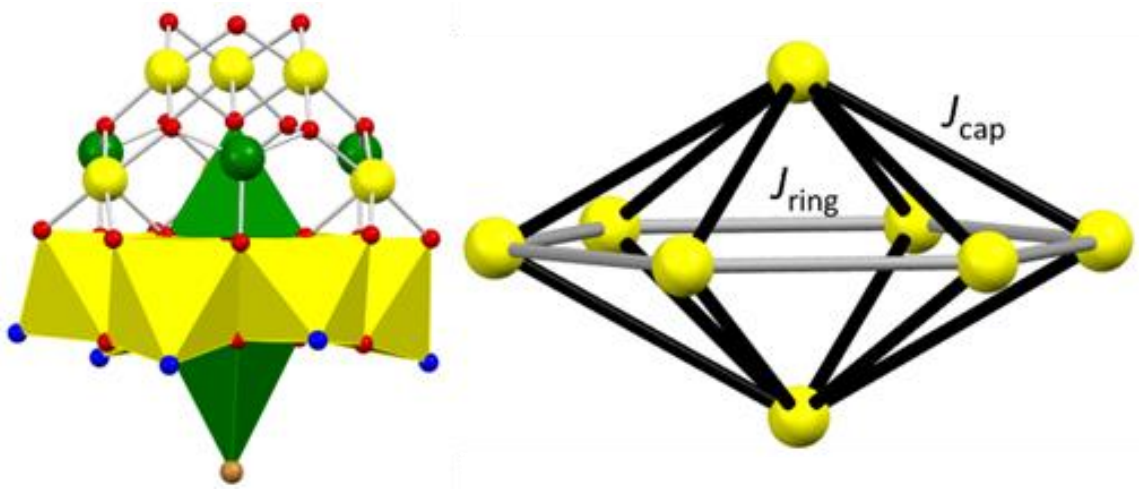

Fig.2 The structure of [Fe_8] in polyhedral format mapped onto half of the [Fe_{17}] cluster represented in ball and stick format (left). The magnetic skeleton of **1** highlighting the two magnetic exchange interactions, J_{cap} and J_{ring} (right).

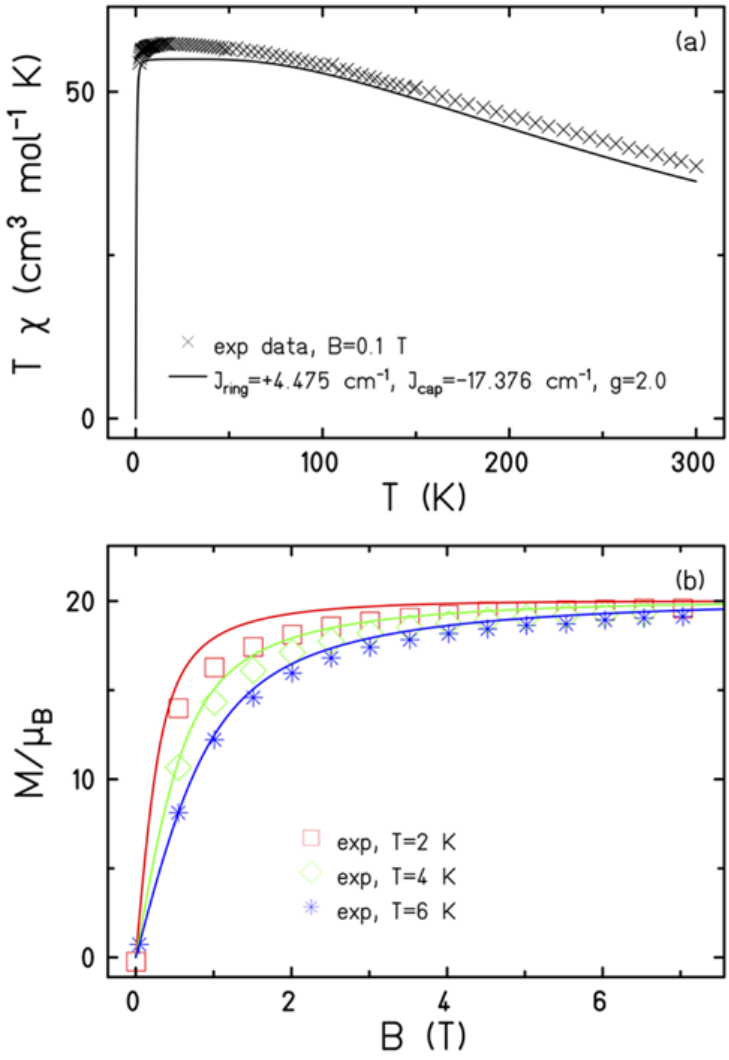

Fig. 3 (a) Plot of the χT product versus T in the 300-2 K temperature range in an applied field, B = 0.1 T. (b) Plot of M versus B in the 2-7 K range for 0.5 ≤ B ≤ 7T. The solid lines represent a fit of the dexperimental data with the indicated parameters. See text for details.

In conclusion, the simple reaction between anhydrous $FeBr_3$ and MeO-py results in the formation of an $[Fe^{III}_8]$ cluster whose metallic skeleton conforms to a hexagonal bipyramid, and whose metal-oxygen core is related to the mineral magnetite. Magnetic measurements reveal antiferromagnetic exchange between the two capping tetrahedral Fe^{III} ions and the six ring octahedral Fe^{III} ions leading to an S = 10 ground state. The ease of synthesis and the striking structural similarity of $[Fe_8]$ to other molecular iron oxides such as $[Fe_{13}]$, $[Fe_{17}]$, $[Fe_{30}]$ and $[Fe_{34}]$ suggests that many more such species with much larger nuclearities remain undiscovered.

Acknowledgements

EKB thanks the EPSRC (EP/V010573/1). MKS would like to thank Edinburgh Compute and Data Facility (ECDF), and the European Union Horizon 2020 research and innovation programme under the Marie Skłodowska-Curie grant agreement No. 832488. For the purpose of open access, the author has applied a Creative Commons Attribution (CC BY) license to any Author Accepted Manuscript version arising from this submission.

Notes and references

H. Weihe and H.U. Güdel, *J. Am. Chem. Soc*., 1998, **120**, 2870–2879.

R. D. Cannon and R. P. White, *Prog. Inorg. Chem*., 1998, **36**, 195-298.

J. K. McCusker, J. B. Vincent, E. A. Schmitt, M. L. Mino, K. Shin, D. K. Coggin, P. M. Hagen, J. C. Huffman, G. Christou and D. N. Hendrickson, *J. Am. Chem. Soc*., 1991, **113**, 3012–302.

C. Cañada-Vilalta, T. A. O'Brien, E. K. Brechin, M. Pink, E. R. Davidson and G. Christou, *Inorg. Chem*., 2004, **43**, 5505–5521.

D. Gatteschi, R. Sessoli and A. Cornia, *Chem. Commun*., 2000, 725-732.

V. O. Garlea, S. E. Nagler, J. L. Zarestky, C. Stassis, D. Vaknin, P. Kögerler, D. F. McMorrow, C. Niedermayer, D. A. Tennant, B. Lake, Y. Qiu, M. Exler, J. Schnack and M. Luban, *Phys. Rev. B*. 2006, **73**, 024414.

a) D. M. Low, L. F. Jones, A. Bell, E. K. Brechin, T. Mallah, E. Rivière, S. J. Teat and E. J. L. McInnes, *Angew. Chem. Int. Ed*., 2003, **115**, 3911-3914; b) R. Shaw, R. H. Laye, L. F. Jones, D. M. Low, C. Talbot-Eeckelaers, Q. Wei, C. J. Milios, S. Teat, M. Helliwell, J. Raftery, M. Evangelisti, M. Affronte, D. Collison, E. K. Brechin and E. J. L. McInnes, *Inorg. Chem*., 2007, **46**, 4968–4978; c) E. Garlatti, S. Carretta, J. Schnack, G. Amoretti and P. Santini, *Appl. Phys. Lett.*, 2013, **103**, 202410.

G. W. Powell, H. N. Lancashire, E. K. Brechin, D. Collison, S. L. Heath, T. Mallah and W. Wernsdorfer, *Angew. Chem. Int. Ed*., 2004, **43**, 5772−5775.

H. Docherty, J. Peng, A. P. Dominey and S. P. Thomas, *Nat. Chem*., 2017, **9**, 595–600.

C. Xie, Y. Duan, W. Xu, H. Zhang, X. Li, Angew. Chem. Int. Ed. 2017, 56, 14953 –14957.

R. A. Revia and M. Zhang, *Mater. Today*, 2016, **19**, 157–168.

a) A. Bino, M. Ardon, D. Lee, B. Spingler and S. J. Lippard, *J. Am. Chem. Soc*., 2002, **124**, 4578−4579; b) J. van Slageren, P. Rosa, A. Caneschi, R. Sessoli, H. Casellas, Y. V. Rakitin, L. Cianchi, F. Del Giallo, G. Spina, A. Bino, A.-L. Barra, T. Guidi, S. Carretta and R. Caciuffo, *Phys. Rev. B*, 2006, **73**, 014422; c) O. Sadeghi, L. N. Zakharov and M. Nyman, *Science*, 2015, **347**, 1359-1362; d) O. Sadeghi, C. Falaise, P. I.

Molina, R. Hufschmid, C. F. Campana, B. C. Noll, N. D. Browning and M. Nyman, *Inorg. Chem*., 2016, **55**, 11078−11088; e) N. A. G. Bandeira, O. Sadeghi, T. J. Woods, Y.-Z. Zhang, J. Schnack, K. R. Dunbar, M. Nyman and C. Bo, *J. Phys. Chem. A*, 2017, **121** 1310-1318.

a) C. Vecchini, D. H. Ryan, L. M. D. Cranswick, M. Evangelisti, W. Kockelmann, P. G. Radaelli, A. Candini, M. Affronte, I. A. Gass, E. K. Brechin and O. Moze, *Phys. Rev. B*, 2008, 77, 224403; b) M. Evangelisti, A. Candini, A. Ghirri, M. Affronte, G. W. Powell, I. A. Gass, P. A. Wood, S. Parsons, E. K. Brechin, D. Collison and S. L. Heath, *Phys. Rev. Lett*., 2006, **97**, 167202; c) I. A. Gass, C. J. Milios, M. Evangelisti, S. L. Heath, D. Collison, S. Parsons and E. K. Brechin, *Polyhedron*, 2007, **26**, 1835–1837; e) I. A. Gass, E. K. Brechin and M. Evangelisti, *Polyhedron*, 2013, **52**, 1177-1180.

A. E. Dearle, D. J. Cutler, M. Coletta, E. Lee, S. Dey, S. Sanz, H. W. L. Fraser, G. S. Nichol, G. Rajaraman, J. Schnack, L. Cronin and E. K. Brechin, *Chem. Commun*., 2022, **58**, 52-22.

A. E. Dearle, D. J. Cutler, H. W. L. Fraser, S. Sanz, E. Lee, S. Dey, I. F. Diaz-Ortega, G. S. Nichol, H. Nojiri, M. Evangelisti, G. Rajaraman, J. Schnack, L. Cronin and E. K. Brechin, *Angew. Chem. Int. Ed*., 2019, **58**, 16903-16906.

a) M. T. Pope and A. Müller, *Angew. Chem., Int. Ed. Engl*., 1991, **30** , 34-48; b) H. N. Miras, J. Yan, D.-L. Liang and L. Cronin, *Chem. Soc. Rev*., 2012, **41**, 7403-7430.

X.-Y. Zheng, H. Zhang, Z. Wang, P. Liu, M.-H. Du,Y.-Z. Han, R.-J. Wei, Z.-W. Ouyang, X.-J. Kong, G.i-L. Zhuang, L.-S. Long and L.-S. Zheng, *Angew. Chem. Int. Ed*., 2017, **56**, 11475-11479.

a) K. Bärwinkel, H.-J. Schmidt and J. Schnack, *J. Magn. Magn. Mater*., 2000, **212**, 240-250; b) R. Schnalle and J. Schnack, *Int. Rev. Phys. Chem*., 2010, **29**, 403-452; c) T. Heitmann and J. Schnack, *Phys. Rev. B*, 2019, **99**, 134405.

a) M. K. Singh and G. Rajaraman, *Inorg. Chem*., 2019, **58**, 3175-3188; b) D. J. Cutler, M. K. Singh, G. S. Nichol, M. Evangelisti, J. Schnack, L. Cronin and E. K. Brechin, *Chem. Commun*., 2021, **57**, 8925-8928.

a) M. Coletta, T. G. Tziotzi, M. Gray, G. S. Nichol, M. K. Singh, C. J. Milios and E. K. Brechin, *Chem. Commun*., 2021, **57**, 4122-4125; b) M. K. Singh, *Dalton Trans*., 2020, **49**, 4539-4548; c) M. Coletta, S. Sanz, D. J. Cutler, S. J. Teat, K. J. Gagnon, M. K. Singh, E. K. Brechin and S. J. Dalgarno, *Dalton Trans*., 2020, **49**, 14790-14797; d) M. K. Singh, T. Rajeshkumar, R. Kumar, S. K. Singh and G. Rajaraman, *Inorg. Chem*., 2018, **57**, 1846-1858; e) M. K. Singh, N. Yadav and G. Rajaraman, *Chem. Commun*., 2015, **51**, 17732-17735.

Supporting Information

Synthesis

All manipulations were performed under aerobic conditions, using materials as received. 4-methoxypyridine (CAS RN: 620-08-6, 98.00%, Fluorochem), $FeBr_3$ (CAS RN: 10031-26-2, 98%, Fluorochem), Acetone (99.8%, Merck). Elemental analyses (C, H, N) were performed by The University of Edinburgh, School of GeoSciences microanalysis service.

$[Fe^{III}_8(\mu_3\text{-}O)_6(\mu\text{-}OH)_6(4\text{-}MeOpy)_{12}Br_2]Br_4\cdot(4\text{-}MeOpy)$ (1)

$FeBr_3$ (2 mmol, 0.591 g) was dissolved in 4-methoxypyridine (4-MeOpy, 200 mmol, 20 ml). The resulting dark orange solution was stirred at room temperature for 2.5 hours, before being filtered. Vapour diffusion of acetone into the filtrate resulted in plate-shaped orange crystals suitable for single crystal X-ray diffraction. Yield: ≤ 10%. Elemental analysis: C, 36.84 (36.65); H, 3.84 (4.15); N, 7.16 (7.17).

Single Crystal and Powder X-ray diffraction

A suitable crystal with dimensions 0.12 × 0.06 × 0.02 mm^3 was selected and mounted on a MITIGEN holder in perfluoroether oil on a Rigaku FRE+ equipped with VHF Varimax confocal mirrors and an AFC12 goniometer and HyPix 6000 detector. The crystal was kept at a steady T = 100(2) K during data collection. The structure was solved with the ShelXT 2018/2 structure solution program using the dual methods solution method and by using Olex2 1.3 as the graphical interface. The model was refined with version 2018/3 of ShelXL 2018/3 (Sheldrick, 2015) using full matrix least squares minimisation on F^2 minimisation.[1,2] Powder XRD measurements were collected on freshly prepared samples of **1** using a Bruker D2 PHASER with nickel filtered Cu radiation at power 30 kW and current 10mA. Diffraction patterns are measured from 2θ = 5° - 30°; step size, 0.0101°.

Thermogravimetric Analysis

TGA analysis was performed on a Netzsch STA 449F1 instrument with a platinum furnace under a nitrogen atmosphere (20 ml min^{-1}) in the 20 – 900 K temperature range (2 K min^{-1}).

Magnetic Measurements

Variable-temperature, solid-state direct current (dc) magnetic susceptibility data down to 2.0 K were collected on a Quantum Design MPMS-XL SQUID magnetometer equipped with a 7 T DC magnet. The crystalline sample was embedded in eicosane and diamagnetic corrections were applied to the observed paramagnetic susceptibilities.

Table S1: Crystallographic details for compound **1**.

Compound	**1**
Formula	$C_{84}H_{109}Br_6Fe_8N_{14}O_{28.5}$
$D_{calc.}$/ g cm^{-3}	1.717
μ/mm^{-1}	3.457
Formula Weight	2697.11
Colour	orange
Shape	plate-shaped
Size/mm^3	0.12×0.06×0.02
T/K	100(2)
Crystal System	monoclinic
Space Group	$C2/c$
a/Å	24.5496(9)
b/Å	27.2170(10)
c/Å	16.4374(7)
α/°	90
β/°	108.242(4)
γ/°	90
V/Å^3	10430.9(7)
Z	4
Z'	0.5
Wavelength/Å	0.71073
Radiation type	Mo K_α
Θ_{min}/°	1.496
Θ_{max}/°	27.101
Measured Refl's.	80637
Indep't Refl's	11498
Refl's I≥2 σ(I)	8514
R_{int}	0.1172
Parameters	736
Restraints	26
Largest Peak	1.057
Deepest Hole	-0.692
GooF	1.018
wR_2 (all data)	0.1148
wR_2	0.1044
R_1 (all data)	0.0732
R_1	0.0456
CCDC	2163355

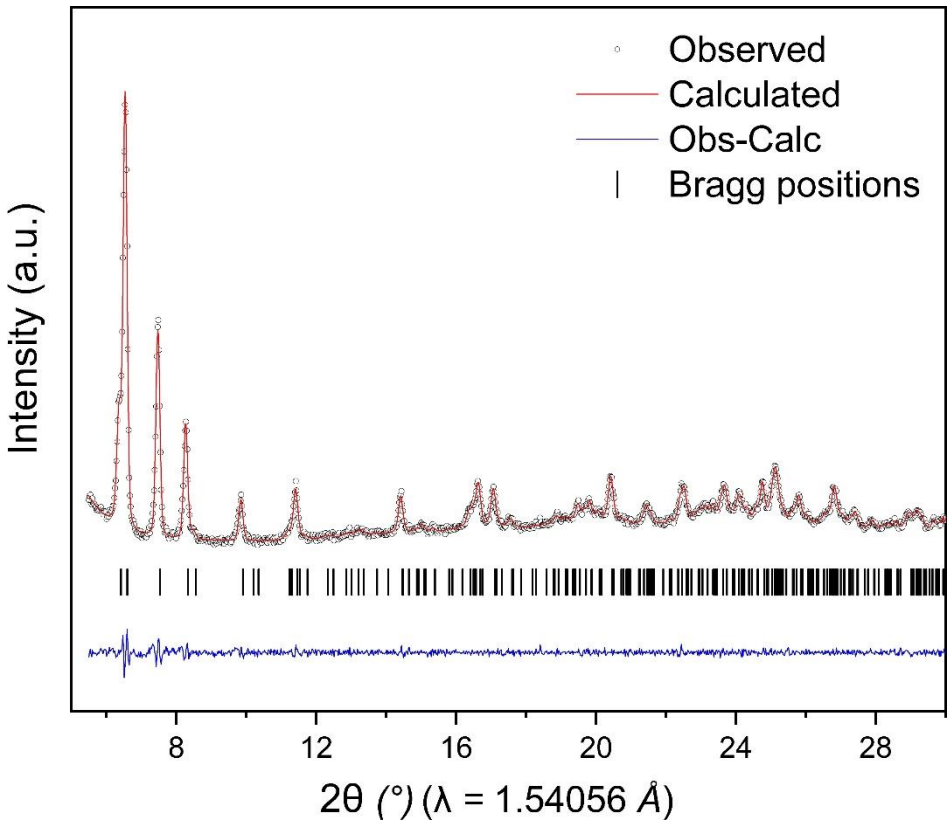

Figure S1. Refinement of the experimental diffraction data of **1** collected at room temperature by using the Le Bail method and the single-crystal structural model as starting parameters. Experimental (black circles), calculated (red line), difference plot [(I_{obs}–I_{calc})] (blue line) and Bragg positions (black ticks). Monoclinic, *C*2/*c*; *a* = 24.6136 Å; *b* = 27.5062 Å; *c* = 16.4066 Å; α = γ = 90°; β = 107.6354 °; R_{exp} = 1.16 %, R_{wp} = 1.72 %, GoF = 1.48.

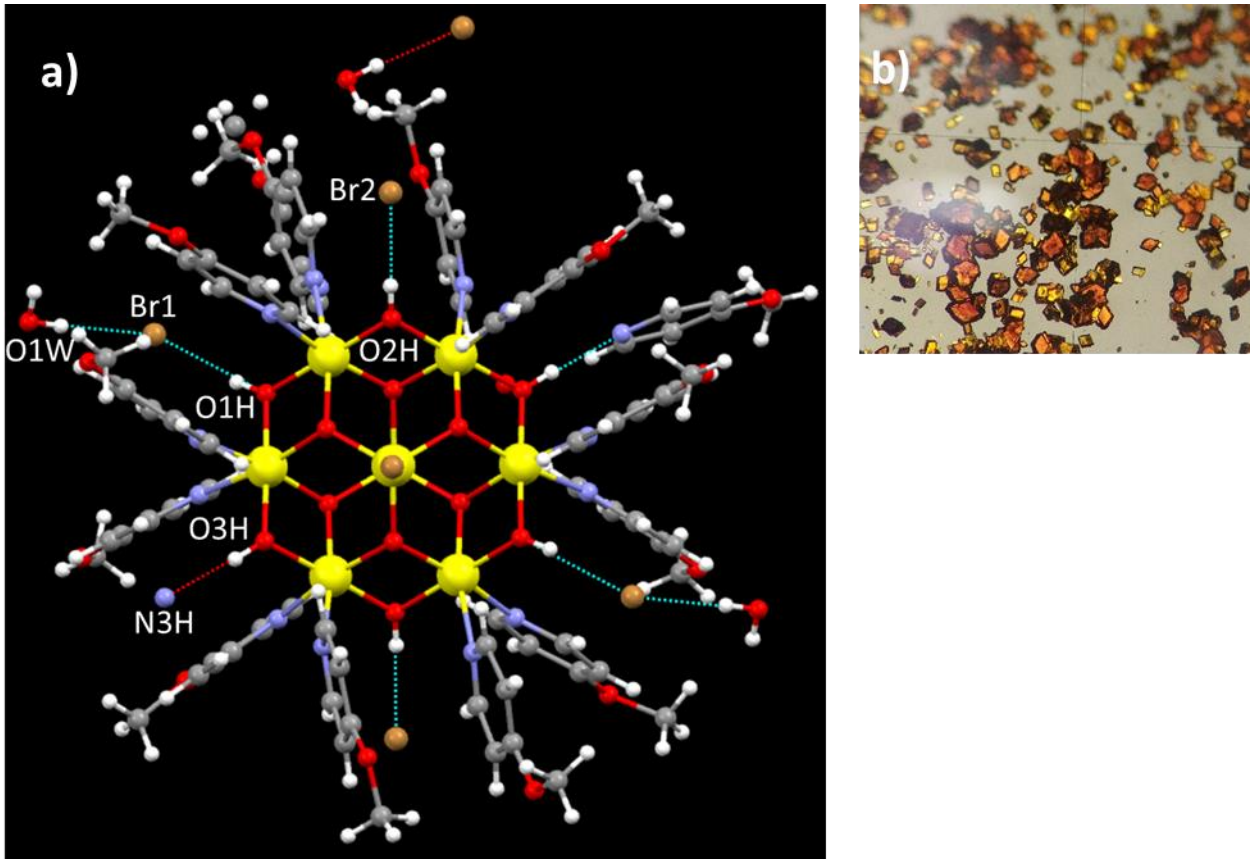

Figure S2. a) H-bonding interactions between the cluster cation of **1**, the Br counter anions and H_2O, Me-OPy molecules of crystallisation. H-bonds are shown as dashed blue lines. Colour code: Fe = yellow, O = red, C = grey, N = blue, H = white, Br = brown. b) Microscope image of the crystals of **1**.

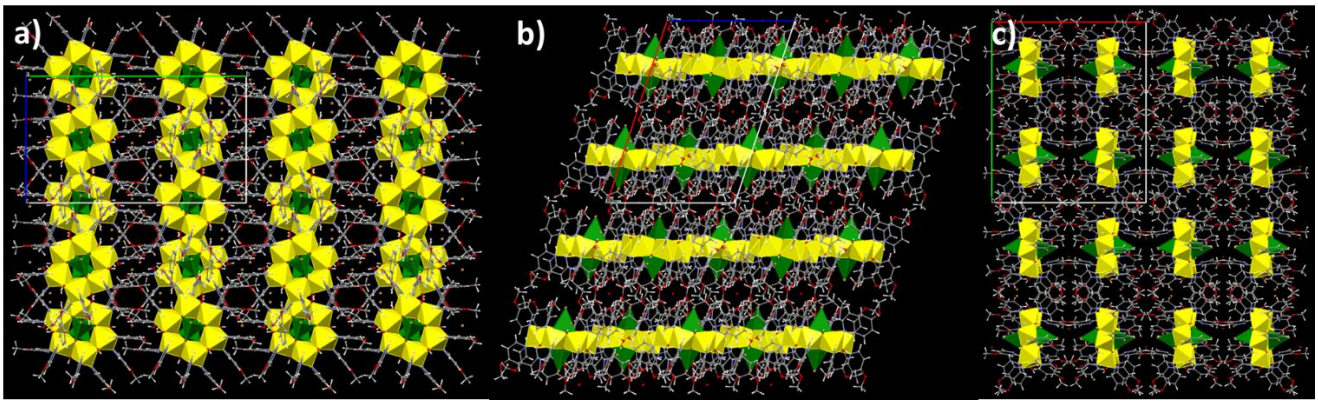

Figure S3. Packing diagram of **1** viewed down the three unit cell axes, respectively, highlighting the layered packing of the cluster cations in the extended structure. The Fe^{III} ions are shown in polyhedral format with octahedral ions in yellow and tetrahedral ions in green.

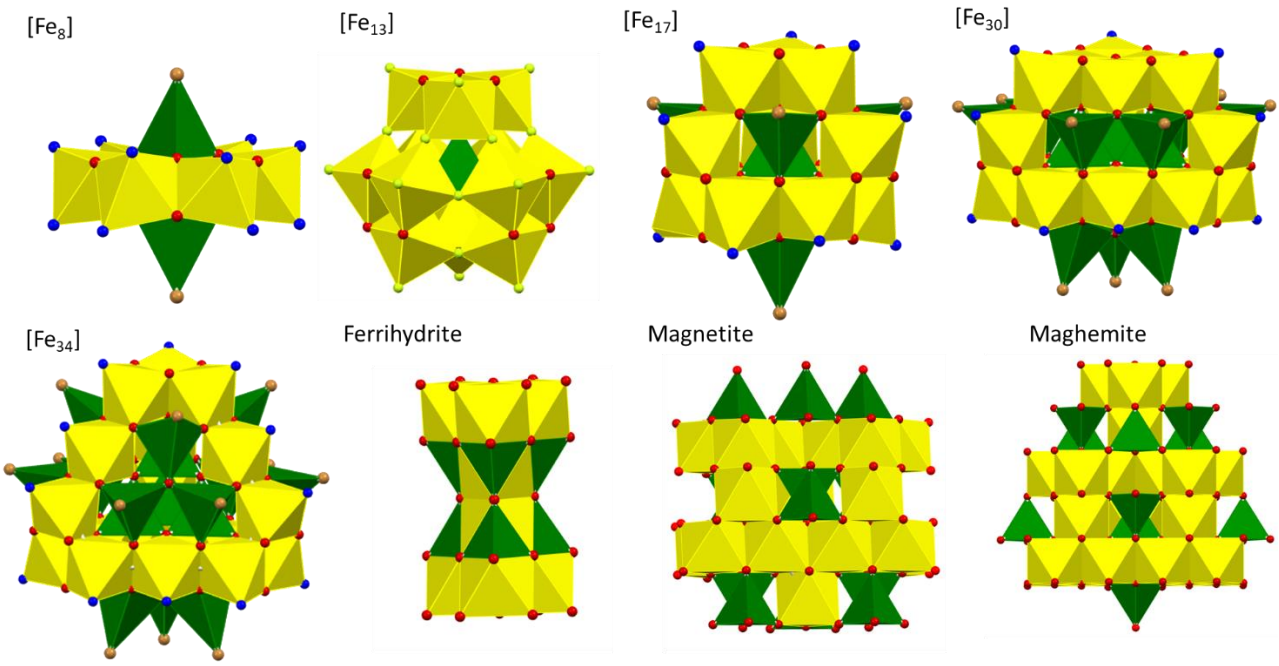

Figure S4. A structural comparison of the structures of [Fe_8], [Fe_{13}], [Fe_{17}], [Fe_{30}], [Fe_{34}], magnetite, maghemite and ferrihydrite.

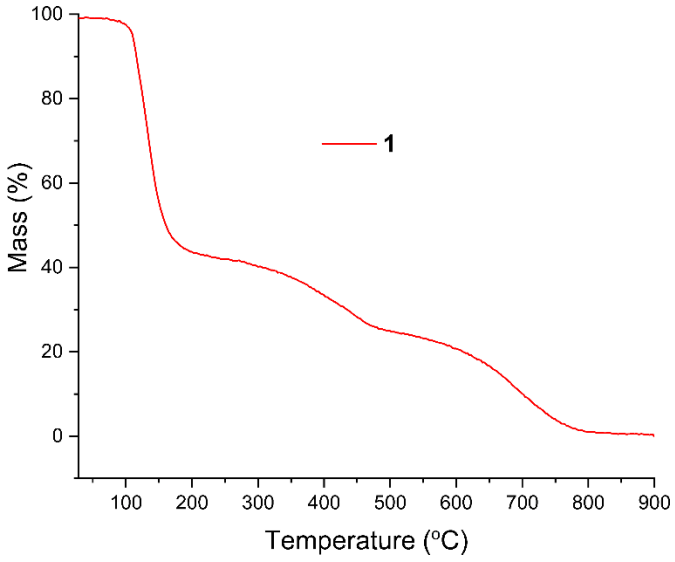

Figure S5. Thermogravimetric analysis of **1** (red line) under a nitrogen flow of 20 ml min^{-1} and heating rate 2 °C min^{-1}. The weight loss of 39 % below 111 °C corresponds to the loss of ten 4-methoxypyridine molecules.

Computational Details

For the DFT calculations we have used the Gaussian 09 suite[3] of programs to estimate the magnetic exchange coupling constants J_{ring} and J_{cap} (where J_{ring} is the interaction between Fe_{oct}-Fe_{oct} and J_{cap} is the interaction between Fe_{oct}-Fe_{tet}) using two sets of calculations. For the first set of calculations, we have used pairwise exchange interaction calculations keeping only the two paramagnetic centres of interest, and replacing the remaining six paramagnetic ions with Ga^{III} ions (Models **1A** and **1B**). For the second set of calculations, we have kept two adjacent Fe_{Oct} centres and one Fe_{tet} centre, replacing the remaining five Fe^{III} ions with five diamagnetic Ga^{III} ions (Model **1C**). For **1C**, we have calculated one high spin configuration with all three Fe^{III} spins up (S = 15/2) and three broken symmetry configurations with one of the Fe^{III} centres spin down (S = 5/2). We have employed the hybrid B3LYP functional,[4] along with the TZV basis set for Fe, the SVP basis set for Ga, O, N, and the SV basis set for C and H.[5] Density Functional Theory (DFT), together with Noodleman's broken symmetry[6] approach, is established as a reliable methodology for estimating exchange interactions with high accuracy.[7] Overlap integral calculations between non-orthogonal singly occupied molecular orbitals of Fe^{III} centres have been performed to analyse the sign and magnitude of magnetic exchange parameter.[7]

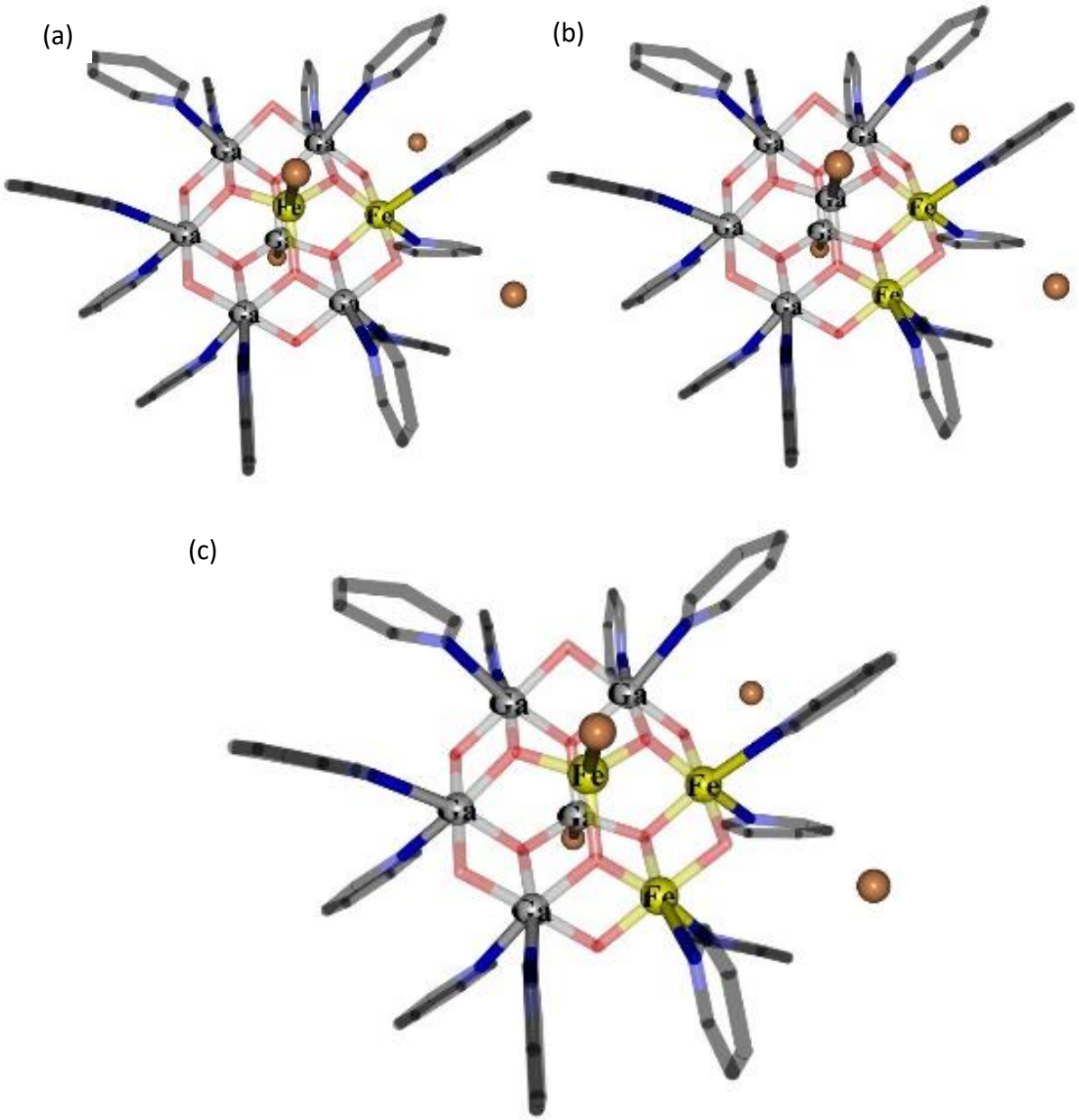

Figure S6. Dimeric models **1A** (a) and **1B** (b), and trimeric model **1C** (c) used for estimating J_{ring} (Fe_{oct}-Fe_{oct}) and J_{cap} (Fe_{oct}-Fe_{tet}).

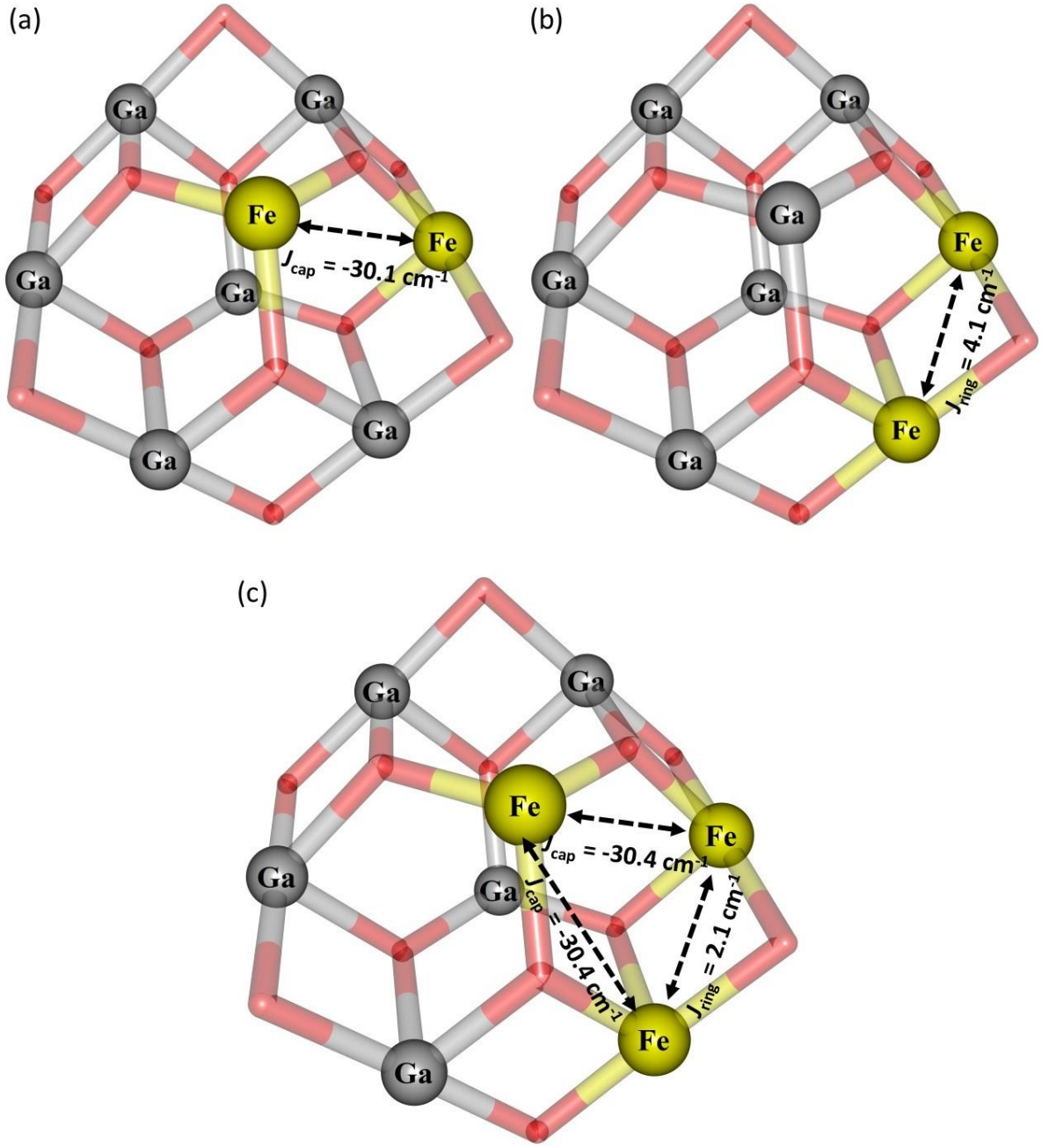

Figure S7. DFT estimated J_{ring} (Fe_{Oct}-Fe_{Oct}) and J_{cap} (Fe_{Oct}-Fe_{Tetr}) magnetic exchange interactions employing the dimeric models **1A** (a) and **1B** (b), and the trimeric model **1C** (c). Note that for model **1C** the errors found for both exchange interactions are less than 0.1.

Table S2. DFT estimated overlap integrals for the dimeric models **1A** and **1B** used to calculate J_{ring} (Fe_{oct}-Fe_{oct}) and J_{cap} (Fe_{oct}-Fe_{tet}). The red value indicates strong magnetic orbital overlap, whereas the green values suggest moderate magnetic orbital overlaps. Black numbers represent orthogonal/weak magnetic orbital overlaps. Note that stronger antiferromagnetic exchange interactions are observed between paramagnetic centres with a larger number of strong or moderate overlap integrals, and vice versa.

J_{ring}	$Fe_{oct}(\alpha)$	d_{yz}	d_{xy}	d_{xz}	$d_{x^2-y^2}$	d_{z^2}
$Fe_{oct}(\beta)$	d_{yz}	0.055	0.017	0.011	0.070	0.008
	d_{xy}	0.028	0.021	0.030	0.040	0.041
	d_{xz}	0.028	0.036	0.040	0.056	0.030
	$d_{x^2-y^2}$	0.007	0.035	0.047	0.014	0.015
	d_{z^2}	0.008	0.001	0.013	0.015	0.001

J_{cap}	$Fe_{tet}(\alpha)$	d_{yz}	d_{xz}	d_{z^2}	d_{xy}	$d_{x^2-y^2}$
$Fe_{oct}(\beta)$	d_{yz}	0.079	0.064	0.054	0.023	0.034
	d_{xy}	0.048	0.087	0.000	0.093	0.070
	d_{xz}	0.056	0.006	0.047	0.010	0.006
	$d_{x^2-y^2}$	0.045	0.001	0.066	0.056	0.099
	d_{z^2}	0.004	0.013	0.023	0.042	0.050

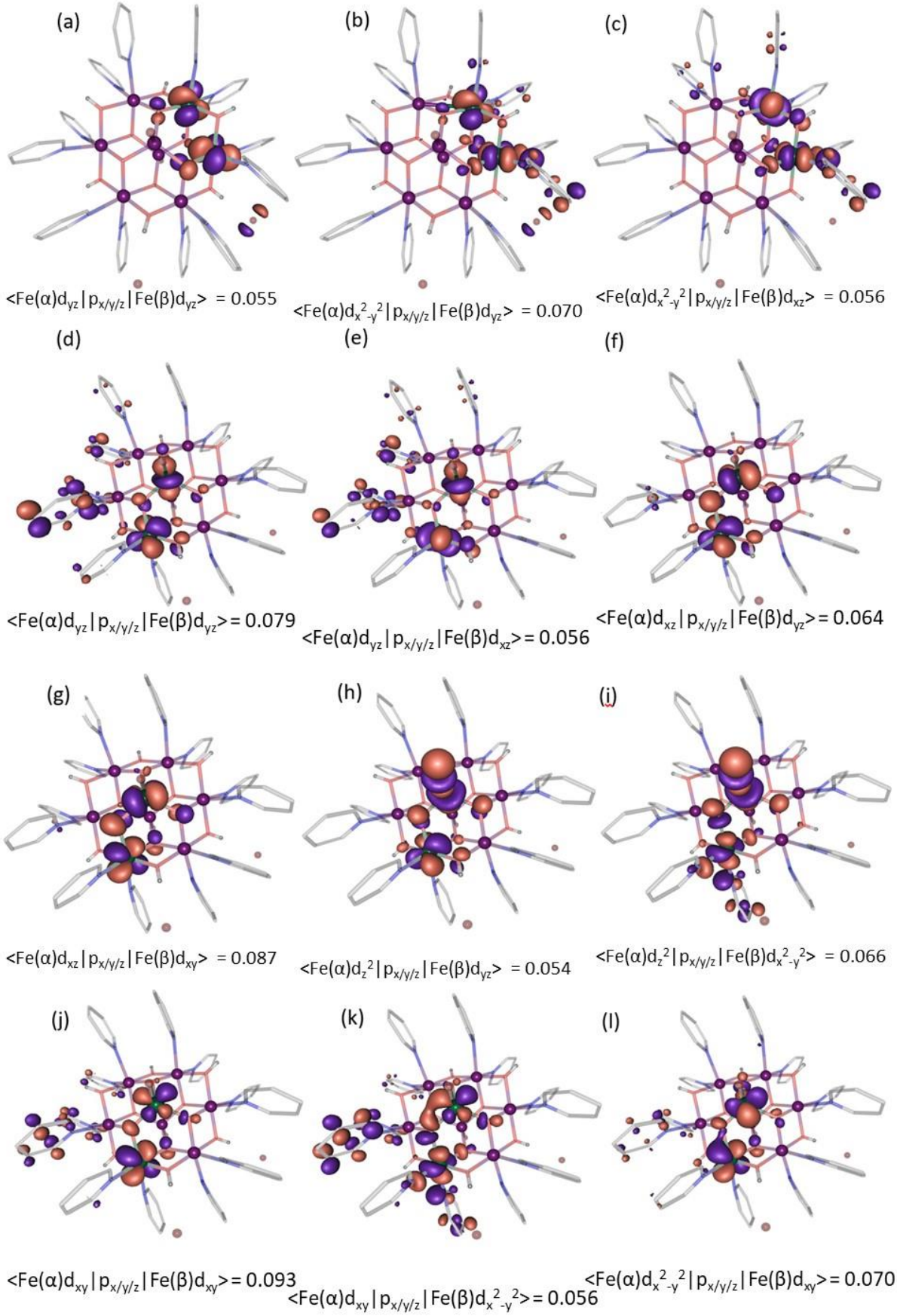
(a)
(b)
(c)
<Fe(α)d$_{yz}$|p$_{x/y/z}$|Fe(β)d$_{yz}$> = 0.055
<Fe(α)d$_{x^2-y^2}$|p$_{x/y/z}$|Fe(β)d$_{yz}$> = 0.070
<Fe(α)d$_{x^2-y^2}$|p$_{x/y/z}$|Fe(β)d$_{xz}$> = 0.056
(d)
(e)
(f)
<Fe(α)d$_{yz}$|p$_{x/y/z}$|Fe(β)d$_{yz}$> = 0.079
<Fe(α)d$_{yz}$|p$_{x/y/z}$|Fe(β)d$_{xz}$> = 0.056
<Fe(α)d$_{xz}$|p$_{x/y/z}$|Fe(β)d$_{yz}$> = 0.064
(g)
(h)
(i)
<Fe(α)d$_{xz}$|p$_{x/y/z}$|Fe(β)d$_{xy}$> = 0.087
<Fe(α)d$_{z^2}$|p$_{x/y/z}$|Fe(β)d$_{yz}$> = 0.054
<Fe(α)d$_{z^2}$|p$_{x/y/z}$|Fe(β)d$_{x^2-y^2}$> = 0.066
(j)
(k)
(l)
<Fe(α)d$_{xy}$|p$_{x/y/z}$|Fe(β)d$_{xy}$> = 0.093
<Fe(α)d$_{xy}$|p$_{x/y/z}$|Fe(β)d$_{x^2-y^2}$> = 0.056
<Fe(α)d$_{x^2-y^2}$|p$_{x/y/z}$|Fe(β)d$_{xy}$> = 0.070

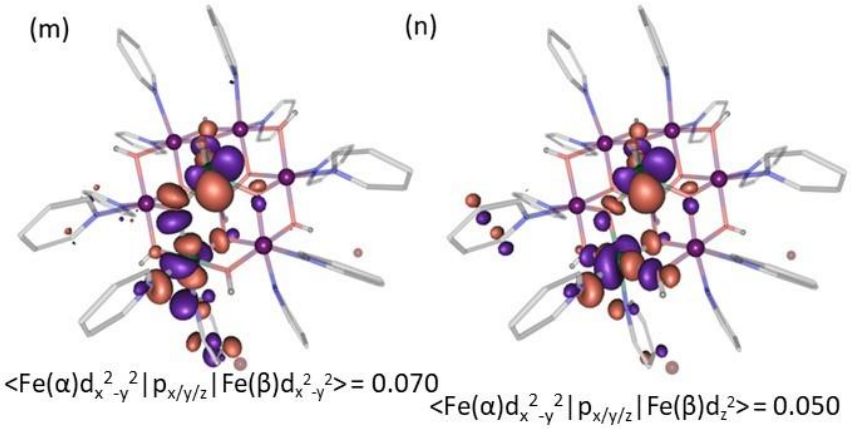

Figure 8. Representative overlap integrals showing strong and moderate Fe^{III} based SOMO(s)-SOMO(s) overlap interactions for J_{ring} (Fe_{oct}-Feo_{ct}) (**a-c**) and J_{cap} (Fe_{Oct}-Fe_{Tetr}) (**d-n**).

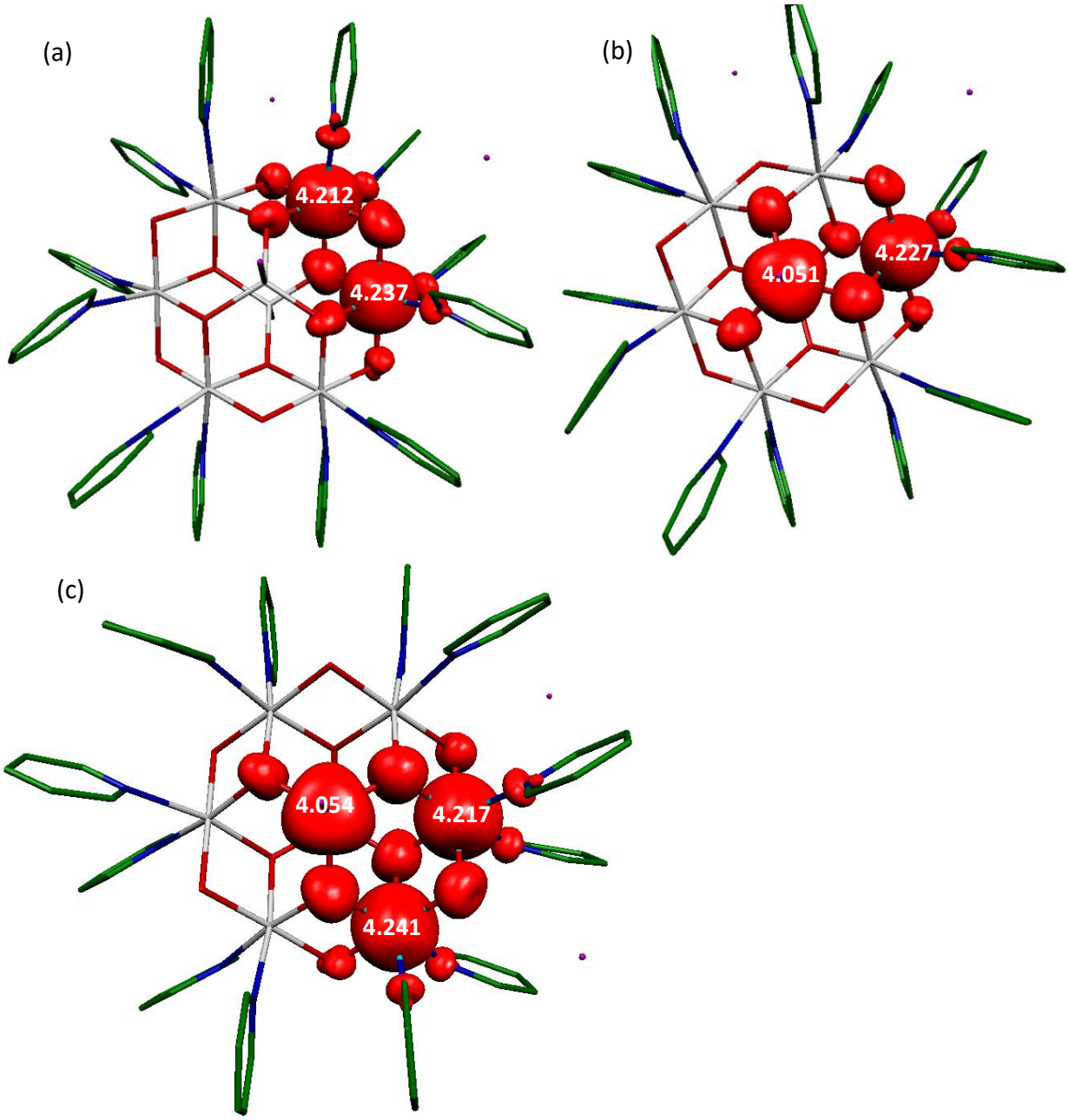

Figure 9. DFT computed spin density plots for models **1A** (a)**, 1B** (b) and **1C** (c). The iso-density surfaces shown corresponds to a value of 0.01 e^{-}/bohr^3. The spin density plots indicate a strong spin delocalization mechanism, with spin density values on the Fe^{III} ions between 4.051 - 4.241. The largest spin density is detected on μ_3-O atoms.

References

1. G. M. Sheldrick, *Acta Crystallogr. Sect. C: Cryst. Struct. Commun.,* 2015, **71**, 3-8.

2. O. V. Dolomanov, L. J. Bourhis, R. J. Gildea, J. A. K. Howard and H. Puschmann, *J. Appl. Crystallogr.,* 2009, **42**, 339-341.

3. M. J. Frisch, G. W. Trucks, H. B. Schlegel, G. E. Scuseria, M. A. Robb, J. R. Cheeseman, G. Scalmani, V. Barone, B. Mennucci, G. A. Petersson, H. Nakatsuji, M. Caricato, X. Li, H. P. Hratchian, A. F. Izmaylov, J. Bloino, G. Zheng, J. L. Sonnenberg, M. Hada, M. Ehara, K. Toyota, R. Fukuda, J. Hasegawa, M. Ishida, T. Nakajima, Y. Honda, O. Kitao, H. Nakai, T. Vreven, J. A. Montgomery, Jr., J. E. Peralta, F. Ogliaro, M. Bearpark, J. J. Heyd, E. Brothers, K. N. Kudin, V. N. Staroverov, T. Keith, R. Kobayashi, J. Normand, K. Raghavachari, A. Rendell, J. C. Burant, S. S. Iyengar, J. Tomasi, M. Cossi, N. Rega, J. M. Millam, M. Klene, J. E. Knox, J. B. Cross, V. Bakken, C. Adamo, J. Jaramillo, R. Gomperts, R. E. Stratmann, O. Yazyev, A. J. Austin, R. Cammi, C. Pomelli, J. W. Ochterski, R. L. Martin, K. Morokuma, V. G. Zakrzewski, G. A. Voth, P. Salvador, J. J. Dannenberg, S. Dapprich, A. D. Daniels, O. Farkas, J. B. Foresman, J. V. Ortiz, J. Cioslowski, and D. J. Fox, Gaussian 09, Revision E.01, Wallingford CT, 2013.

4. a) A. D. Becke, *Phys. Rev. A* 1988, *38*, 3098-3101; b) A. D. Becke, *J. Chem. Phys.,* 1993, **98**, 5648; c) C. Lee, W. Yang, R. G. Parr, *Phys. Rev. B,* 1988, **37**, 785.
5. a) A. Schäfer, H. Horn, R. Ahlrichs, *J. Chem. Phys.,* 1992, **97**, 2571-2577; b) A. Schäfer, C. Huber, R. Ahlrichs, *J. Chem. Phys.,* 1994, **100**, 5829; c) G. E. Scuseria, H. F. Schäfer, *J. Chem. Phys.,* 1989, **90**, 3700.
6. L. Noodleman, *J. Chem. Phys,.* 1981, **74**, 5737.

7. a) M. K. Singh, *Dalton Trans.,* 2020, **49**, 4539-4548; b) M. K. Singh, G. Rajaraman, *Inorg. Chem.,* 2019, **58**, 3175-3188; c) M. K. Singh, G. Rajaraman, *Chem. Eur. J.,* 2015, **21**, 980-983; d) J. Caballero-Jiménez, F. Habib, D. Ramírez-Rosales, R. Grande-Aztatzi, G. Merino, I. Korobkov, M. K. Singh, G. Rajaraman, Y. Reyes-Ortega, M. Murugesu, *Dalton Trans.,* 2015, **44**, 8649; e) C. McDonald, S. Sanz, E. K. Brechin, M. K. Singh, G. Rajaraman, D. Gaynor, L. F. Jones, *RSC Adv.,* 2014, **4**, 38182. f) A. E. Dearle, D. J. Cutler, H. W. L. Fraser, S. Sanz, E. Lee, S. Dey, I. F. Diaz-Ortega, G. S. Nichol, H. Nojiri, M. Evangelisti, G. Rajaraman, J. Schnack, L. Cronin, E. K. Brechin, *Angew. Chem. Int. Ed.,* 2019, **58**, 16903-16906; g) M. Coletta, T. G. Tziotzi, M. Gray, G. S. Nichol, M. K. Singh, C. J. Milios, E. K. Brechin, *Chem. Commun.,* 2021, **57**, 4122-4125; h) D. J. Cutler, M. K. Singh, G. S. Nichol, M. Evangelisti, J. Schnack, L. Cronin, E. K. Brechin, *Chem. Commun.,* 2021, **57**, 8925-8928.